Journal of
Materials Chemistry A

Accepted Manuscript

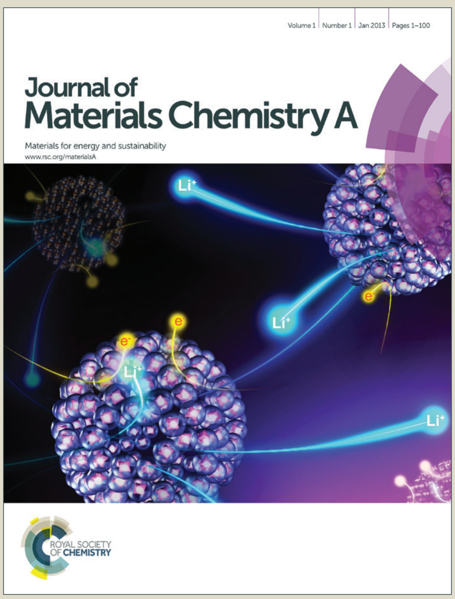

ROYAL SOCIETY
OF CHEMISTRY

www.rsc.org/materialsA

Journal Name

Journal of Materials Chemistry A

Dynamic Article Links ►

Cite this: DOI: 10.1039/c0xx00000x

www.rsc.org/xxxxxx

Communication

The Assembly of Vanadium (IV)-Substituted Keggin-type Polyoxometalate/Graphene Nanocomposite and its application in photovoltaic system

Dan Xu, Wei-Lin Chen*, Jian-Sheng Li, Xiao-Jing Sang, Ying Lu, Zhong-Min Su and En-Bo Wang*

Received (in XXX, XXX) Xth XXXXXXXXX 20XX, Accepted Xth XXXXXXXXX 20XX
DOI: 10.1039/b000000x

The $SiW_{11}V$/graphene nanocomposite was firstly prepared and introduced into the TiO_2 film. It showed a significant photocurrent response, which can be attributed to the photoinduced electrons of $SiW_{11}V$. This work provides a promising strategy for exploring POMs sensitizer with a lower energy level than the CB of TiO_2.

Polyoxometalates (POMs) are a typical class of transition metal–oxygen clusters with a variety of structures, element compositions, and functionalities, which have received extensive attention owing to their excellent properties.[1] POMs can undergo a stepwise multi-electron reversible redox process without any structure changes.[2] In addition, the absorption spectra of POMs can be regulated by introducing multiple transition metal elements, which can even cover as much as the whole UV-Visible light spectrum.[3] Recently, POMs have represented great potentials to apply in the Dye-sensitized solar cells (DSSCs) as the photosensitizers,[4] furthermore, POMs are usually acted as the electron acceptor in the solar photovoltaic system, owing to their lower LUMO (lowest unoccupied molecular orbital) energy level than the CB (conduction band) of TiO_2.[5] Therefore, it is of great significance to explore alternative methods for effectively transferring the photoinduced electrons of POMs.

Graphene, a 2D carbon nanomaterial, which has attracted considerable attentions owing to its high surface area, extraordinary electronic properties, electron transport capabilities and high mechanical and thermal properties.[6,7] Furthermore, graphene has an unusual feature that its band gap is exactly zero.[8] The surface functional groups and lattice defects in graphene sheets can help to anchor and immobilize nanoparticles on it, and the stability of nanoparticles can be improved by dispersing on graphene.[9] So graphene is the unique candidate as 2-D catalyst support due to these advantageous structural and physicochemical properties. Graphene has been introduced into the photoanode of DSSCs since the energy level of graphene is between the CB of TiO_2 and FTO, the 2D graphene behave as an electron transfer channel in the photoanode, which brought a faster electron transformation and a lower recombination.[10, 11]

Herein, graphene may be the promising support for POMs, owing to its low energy level and fast electron transport property, which may transport the photoinduced electrons of POMs rapidly and effectively. Graphene oxide (GO) is a precursor for POM/graphene nanocomposites synthesized by various reduction methods, such as UV photoreduction, electrochemical reduction, chemical reduction fabrication methods, and so on.[12-14] The α-Keggin-type polyoxometalates ($H_4SiW_{12}O_{40}$, $H_3PW_{12}O_{40}$ and $H_3PMo_{12}O_{40}$) are always used in the reduction processes, attributed to their high stability and appropriate redox properties.[12,13] POM/graphene nanocomposites have exhibited promising potential to apply in the photovoltaic system. However, it is worth noting that the light responses of the above POMs are limited to UV light. Thus, a vanadium (IV)-substituted α-Keggin-type polyoxometalate $(SiW_{11}V^{IV}O_{40})^{6-}$ ($SiW_{11}V$) was chosen to load on graphene, the absorption spectrum of which could cover as much as the full spectrum. L-ascorbic acid (L-AA) has a mild reductive ability, which has been used to prepare water soluble reduced GO (RGO).[15] POMs can also be easily reduced by some mild reducing agents, such as L-AA and zinc powder.[16] Therefore, L-AA was chosen as the appropriate reductant in our case.

In this paper, $SiW_{11}V$/graphene nanocomposite is prepared by a simple two-step chemical reduction approach at room temperature, which is a facile and friendly environmental method. As shown in Fig. 1, in the first step, $SiW_{11}V$ is reduced by mild reducing agents (L-AA and zinc powder), then the heteropoly blue (HPB) solution react with GO to assemble $SiW_{11}V$ clusters on the graphene sheets. Otherwise, the excess L-AA in the first step can also reduce GO, in this system, L-AA is the recductant for both $SiW_{11}V$ and GO. Herein, the $SiW_{11}V$/graphene nanocomposites were introduced into the TiO_2 films, the photovoltaic performance of the composite films was investigated by photocurrent transient measurements, the photocurrent responses of which have a significant increase compared with the blank TiO_2 particle film. As far as we know, it is the first time that $SiW_{11}V$/graphene nanocomposite is prepared and introduced into the TiO_2 film.

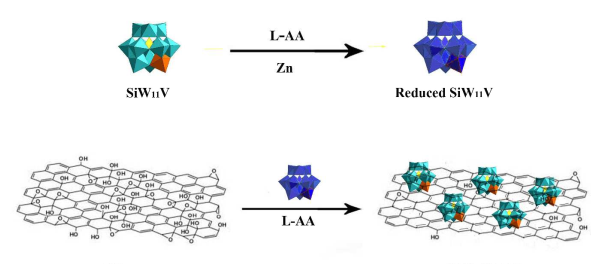

Fig. 1 The process of the assembly of $SiW_{11}V$/grapheme nanocomposite.

GO, $K_6[SiW_{11}V^{IV}O_{40}]\cdot 7H_2O$ and $SiW_{11}V$/graphene nanocomposites were prepared (for details see ESI), GO and $K_6[SiW_{11}V^{IV}O_{40}]\cdot 7H_2O$ were characterized by Fourier transform infrared (FTIR) (Fig. S1 and S2). The reduction of GO and the assembly of $SiW_{11}V$ clusters on the RGO sheets were confirmed by the X–ray powder diffractions (XRD). Fig. S3 shows the XRD patterns of raw graphite (a), GO (b), RGO (c), $SiW_{11}V$ (d) and $SiW_{11}V$/grapheme-3 (e). The raw graphite shows a strong peak at $2\theta = 26.5°$, corresponding to a *d*-spacing of 3.36 Å. As for GO, the peak of graphite is absent, while a new peak at $2\theta = 11.8°$ is arisen, which is consistent with an average interlayer spacing of 7.49 Å. Since GO has lots of oxygen-containing functional groups attached on its both sides, so the average interlayer spacing of GO is increased.[17] After the reduction process, there is a broad 002 peak at 23.5°, the interlayer spacing decreases from 7.49 Å of the pristine GO to 3.78 Å, indicating that RGO are successfully obtained. In the pattern of $SiW_{11}V$/graphene-3, the 002 reflection is broader than RGO, suggesting that the order of the $SiW_{11}V$/graphene-3 is very poor along the stacking direction, implying that the sample is mostly composed of single or a few layers of RGO.[17, 18] It also indicates that $SiW_{11}V$ clusters are successfully incorporated into the adjacent graphene sheets. At the same time, the $SiW_{11}V$ does not show the characteristic diffraction patterns in the pattern of $SiW_{11}V$/graphene-3, which implies that $SiW_{11}V$ clusters exist with the dispersed state, but not the crystalline state.[13]

Moreover, the high resolution transmission electron microscope (HRTEM) images and the energy dispersive X-ray spectroscopy (EDS) further indicate that the $SiW_{11}V$ clusters exist in the dispersed state on graphene. The TEM images of RGO and $SiW_{11}V$/graphene-3 (Figs. S4 and 2a) exhibit crumpled and paper-like nanosheet morphology of the samples. In the high magnification HRTEM image of $SiW_{11}V$/graphene-3 (Fig. 2b), $SiW_{11}V$ clusters can be observed clearly as small dark spots, no agglomerate or nanocrystal can be detected, and the size of clusters are around 1−3 nm. Besides that, the $SiW_{11}V$ clusters on the graphene surface are in a uniformly dispersed state, which is consistent with the XRD results. The EDS analysis of $SiW_{11}V$/graphene-3 shows the C, Si, W and V elements can be observed obviously (Fig. S5).

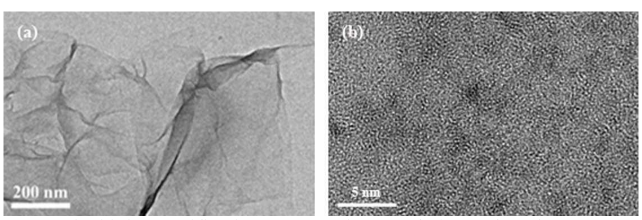

Fig. 2 The high magnification HRTEM image of $SiW_{11}V$/graphene-3.

X-ray photoelectron spectra (XPS) was also used to detect the reduction degree of GO. Fig. 3a shows the C 1s XPS spectra of GO, four types of carbon with different chemical states are observed: 284.6 eV (sp^2 C), 286.7 eV (C–O), 287.7 eV (C=O), and 288.8 eV (O−C=O), respectively. After the reduction, the content of oxygen-containing groups decreases dramatically, especially the peak of C–O (Fig. 3b and 3c). In addition, there is an additional component at 285.4 eV corresponding to sp^3 C in the spectra of $SiW_{11}V$/graphene-3, which reveals that the reduction can effectively remove most oxygen-containing groups.[13] Since $SiW_{11}V$/graphene-3 has less oxygen-containing functional groups than $SiW_{11}V$/graphene-1, the relatively high original concentration of $SiW_{11}V$ may result in a more efficient and deeper reduction of GO. The W4f XPS spectra of $SiW_{11}V$/graphene-3 nanocomposite shown in Fig. 3d indicates that the $W^{VI}4f_{5/2}$ and $W^{VI}4f_{7/2}$ peaks are located at 35.0 eV and 37.1 eV, which are consistent with the W^{VI} oxidation state, indicating the oxidized state form of the POM anions.[19]

Moreover, thermogravimetric analyses (TGA) are carried out to study the significant structural changes occurring during the chemical reduction process, the contents of $SiW_{11}V$ clusters on the $SiW_{11}V$/graphene nanocomposite and the thermal stability of the samples. The thermal stability investigations of $K_6[SiW_{11}V^{IV}O_{40}]\cdot 7H_2O$ (Fig. S6) indicate that there is no significant mass loss observed even heated to 600 °C, suggesting the good thermal stability of the chosen POM.

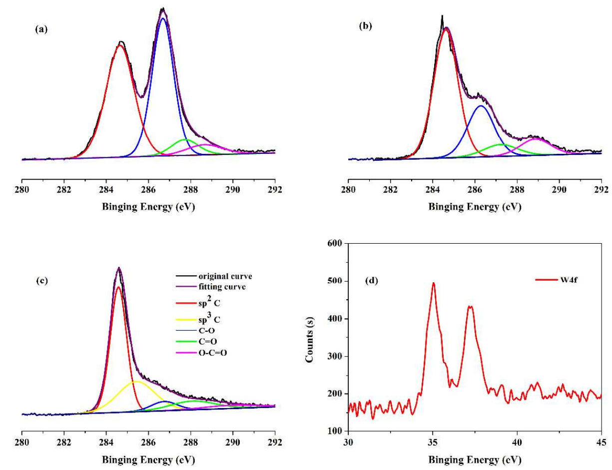

Fig. 3 C 1s XPS spectrum of (a) GO, (b) $SiW_{11}V$/graphene-1 and (c) $SiW_{11}V$/graphene-3; and (d) the XPS spectrum of $SiW_{11}V$/graphene-3 for W4f.

Fig. S7a shows the TGA curves of GO, RGO and $SiW_{11}V$/graphene-3. The first stage of all the samples (20-100 °C) corresponds to the loss of the adsorbed and crystallization water molecules. The second weight loss of GO occurs at *ca.* 200 °C, which corresponds to the loss of labile oxygen-containing functional groups in GO.[20] The final weight loss of GO occurred between 500 and 600 °C is attributed to the combustion of carbon matter.[21] The TG curve of graphene presents the structural change induced by the reduction using L-AA, which also confirms that some oxygen functionalities in the GO are not reduced. However, no significant mass loss of $SiW_{11}V$/graphene-3 is detected, revealing that the most oxygen containing functional groups are removed after the reduction and the thermal stability is increased dramatically. The weight residual of $SiW_{11}V$/graphene-3 has a remarkable increase compared to graphene, which may be caused by the $SiW_{11}V$ assembled on the graphene.

Under the same conditions, the increasing of the original mass of $SiW_{11}V$ results in the increase of the thermal stability and more weight residual for the $SiW_{11}V$/graphene, as shown in Fig. S7b. These observations are consistent with the XPS results (see above), which indicate that the more efficient reduction of GO and more $SiW_{11}V$ assemble on RGO can be realized by the relatively high original mass of $SiW_{11}V$. All the studies confirm that $SiW_{11}V$ clusters have been successfully attached onto the RGO sheets.

POMs have a strong affinity with graphene, which may be attributed to the electron transfer interaction between graphene and POMs and the protonation-induced electrostatic interaction between POMs and the oxygen-containing groups (such as hydroxyl and carboxyl groups) on the surface of graphene. [14, 22, 23, 24] In our case, the former should be the dominating one, because the mass of the loaded $SiW_{11}V$ clusters increasing dramatically and the content of retained oxygen-containing groups decreased remarkably as we increasing the original mass of $SiW_{11}V$. Moreover, the $W^{VI}4f_{5/2}$ and $W^{VI}4f_{7/2}$ peaks of $SiW_{11}V$/graphene-3 nanocomposite (Fig. 3d) shift to lower binding energies compared with those of $SiW_{11}V$ (the $W^{VI}4f_{5/2}$ and $W^{VI}4f_{7/2}$ peaks of $SiW_{11}V$ are located at 35.8 eV and 37.8 eV in Fig. S8), it also indicates that the electron transfer interaction is the dominating affinity between graphene and POMs in $SiW_{11}V$/graphene-3 nanocomposite.[13]

Wang et al. have confirmed that 0.6 wt% GO in the photoanode of DSSCs would get the best efficiency.[10] So 4 mg of GO has been used to prepare the $SiW_{11}V$/graphene nanocomposite, and the composite was introduced into the TiO_2 film (see ESI). The photocurrent response experiments for $SiW_{11}V$/graphene-3@TiO_2 film, RGO@TiO_2 film and pure TiO_2 film were measured at a constant bias of 0 V (Fig. 4a). This investigation was carried out in the presence of 0.1M Na_2SO_4 aqueous solution. The films were exposed under Xe lamp for 20 s and kept in the dark for another 20 s. As shown in Fig. 4a, the photocurrent response of the RGO@TiO_2 is slightly higher than the pure TiO_2 film. However, compared to the pure TiO_2 and RGO@TiO_2, a more 3-fold increase has been observed of the $SiW_{11}V$/graphene-3@TiO_2 film.

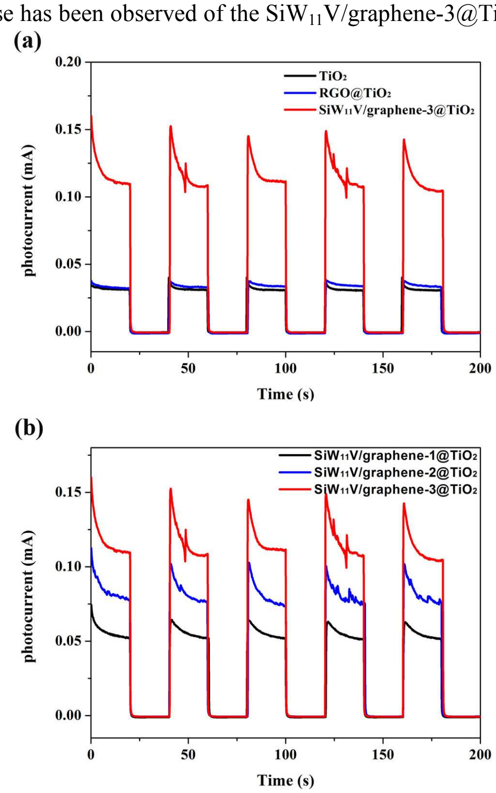

Fig. 4 *I–t* curves for the photocurrent response of the films.

In order to examine the operational principle, the energy levels of all the materials are summarized. The energy levels and band gap of $SiW_{11}V$ can be obtained by the CV and diffuse reflectivity spectra.[4,25] The LUMO of $SiW_{11}V$ is -4.31 eV, which was estimated by the initial reduction potential of $SiW_{11}V$ (-0.19 V *vs* NHE) in the CV curve (Fig. S9). And the band gap could be determined by the plot of Kubelka−Munk function F against energy E, the intersection point between the energy axis and the line extrapolated from the linear portion of the absorption edge is the band gap. As can be seen in Fig. S10, the band gap (E_g) of $SiW_{11}V$ was estimated to be 2.67 eV.

The energy level and electron-transfer processes are illustrated in Scheme 1. It can be seen clearly that the energy level of graphene is between the CB of TiO_2 and FTO, graphene in the RGO@TiO_2 film can transport the photoinduced electrons quickly and suppress the recombination and back electron transfer. However, the RGO@TiO_2 film does not have an apparent increase because TiO_2 can only be excited by UV light. As for $SiW_{11}V$/graphene-3@TiO_2 film, $SiW_{11}V$ has an appropriate band gap, which can be excited by nearly the whole UV-Visible light spectrum, it can be an electrons donor. The LUMO of $SiW_{11}V$ is higher than the energy level of graphene. So the excited electrons of $SiW_{11}V$ can be captured and transported to the FTO rapidly and effectively through the graphene bridges under illumination. On the other hand, $SiW_{11}V$ also act as an electron acceptor and play the role of electron mediator to accelerate the electron transmission and suppress the carrier recombination since the LUMO of $SiW_{11}V$ is lower than the CB of TiO_2. In this system, $SiW_{11}V$ not only acts as an electron acceptor, but also as a sensitizer (electron donor) which has a lower energy level than the CB of TiO_2. Fig. 4b shows the photocurrent responses of $SiW_{11}V$/graphene-*n*@TiO_2 film (n = 1, 2, 3), the photocurrent responses of the films are highly dependent on the mass of $SiW_{11}V$ clusters on graphene, the photocurrent increases gradually with the increasing of the mass of $SiW_{11}V$ clusters. This result is attributed to the more absorbance of the UV-Visible light and more electrons injecting to graphene of the $SiW_{11}V$ clusters.

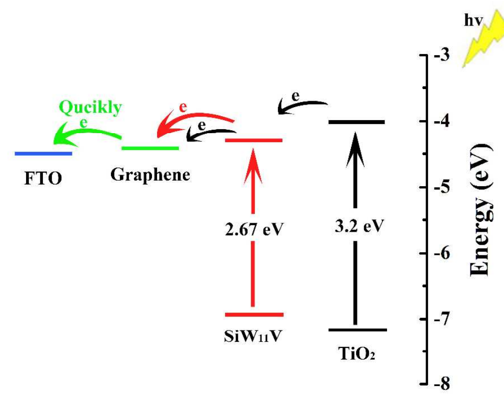

Scheme. 1 Energy level and electron-transfer processes diagram of $SiW_{11}V$/graphene@TiO_2 film.

In summary, it is the first report that the $SiW_{11}V$/graphene nanocomposites have been successfully prepared with a simple two-step chemical reduction approach. And the $SiW_{11}V$/graphene nanocomposite was introduced into the TiO_2 film, which showed a significant photocurrent response. This remarkable increase of the photocurrent response may be attributed to $SiW_{11}V$ can be excited by nearly the full spectrum, and the quick and effective transformation of the photoinduced electrons of $SiW_{11}V$ through the graphene sheets. In this system, $SiW_{11}V$ act as both electron acceptor and electron donor. This work opens a new way for the fabrication of various POM/graphene nanocomposites, and this method is generally suitable for common POMs. Furthermore, it also provides a promising strategy for exploring POMs sensitizer with a lower energy level than the CB of TiO_2.

This work was financially supported by the National Natural Science Foundation of China (no. 21131001 and 21201031), Ph. D station Specialized Research Foundation of Ministry of Education for Universities (no. 20120043120007), Science and

Technology Development Project Foundation of Jilin Province (no. 201201072), and the Testing Foundation of Northeast Normal University.

Notes and references

Department of Chemistry, Key Laboratory of Polyoxometalates Science of Ministry of Education, Northeast Normal University, Changchun, 130024, China. Fax: (+86) 431-85098787, E-mail: wangeb889@nenu.edu.cn, chenwl@nenu.edu.cn

† Electronic Supplementary Information (ESI) available: [details of any supplementary information available should be included here]. See DOI: 10.1039/b000000x/

1 (a) D. L. Long, R. Tsunashima and L. Cronin, *Angew. Chem., Int. Ed.*, 2010, **49**, 1736; (b) J. Hao, Y. Xia, L. S. Wang, L. Ruhlmann, Y.L. Zhu, Q. Li, P. C. Yin, Y. G. Wei, and H. Y. Guo, *Angew. Chem. Int. Ed.*, 2008, **47**, 2626 –2630; (c) B. B. Xu, Z. F. Peng, Y. G. Wei and D. R. Powell, *Chem. Commun.* , 2003, 2562–2563; (d) Z. H. Kang, E. B. Wang, B. D. Mao, Z. M. Su, L. Gao, S. Y. Lian, L. Xu, *J. Am. Chem. Soc.* 2005, ***127***, 6534–6535.

2 M. Sadakane and E. Steckhan, *Chem. Rev.*, 1998, **98**, 219.

3 A. Dolbecq, E. Dumas, C.R. Mayer, P. Mialane, *Chem. Rev.*, 2010, **110**, 6009-6048.

4 (a) X. J. Sang, J. S. Li, L. C. Zhang, Z. J. Wang, W. L. Chen, Z. M. Zhu, Z. M. Su and E. B. Wang, *ACS Appl.Mater Interfaces*, 2014, **6**, 7876−7884; (b) J. S. Li, X. J. Sang, W. L. Chen, L. C. Zhang, Z. M. Su, C. Qin and E. B. Wang, *Inorganic Chemistry Communications*, 2013, 78-82.

5 (a) S. M. Wang, L. Liu, W. L. Chen, E. B. Wang and Z. M. Su, *Dalton Trans.*, 2013, **42**, 2691-2695; (b) Z. X. Sun, F. Y. Li, M. L. Zhao, L X and S F, *Electrochemistry Communications*, 2013, **30**, 38–41.

6 D. Chen, H. Feng and J. Li, *Chem. Rev.,* 2012, **112**, 6027−6053.

7 Y. Zhang, Y. Tan, H. L. Stormer, and P. Kim, *Nature*, 2005, **438**, 201.

8 M. Freitag, *Nat. Nanotechnol.* 2008, ***3***, 455–457.

9 M. M. Liu, R. Z. Zhang, and W. Chen, *Chem. Rev.*, 2014, **114**, 5117–5160.

10 N. L. Yang, J. Zhai, D. Wang, Y. S. Chen and L. Jiang, *ACS Nano*, 2010, **4**, 887–894.

11 (a) Y. B. Tang, C. S. Lee, J. Xu, Z. T. Liu, Z. H. Chen, Z. B. He, Y. L. Cao, G. D. Yuan, H. S. Song, L. Chen, L. B. Luo, H. M. Cheng, W. J. Zhang, I. Bello and S. T. Lee, *ACS Nano*, 2010, **4**, 3482–3488; (b) P. N. Zhu, A. S. Nair, S. J. Peng, S. Y. Yang and S. Ramakrishna, *ACS Appl. Mater. Interfaces*, 2012, **4**, 581−585; (c) G. Zhu, T. Xu, T. Lv, L. K. Pan, Q. F. Zhao, Z. Sun, *Journal of Electroanalytical Chemistry*, 2011, **650**, 248–251; (d) S. R. Sun, L. Gao and Y. Q. Liu, *Applied Physics Letters*, 2010, **96**, 083113; (e) T. H. Tsai, S. C. Chiou and S. M. Chen, *Int. J. Electrochem. Sci.,* 2011, **6**, 3333 – 3343.

12 (a) H. L. Li, S. P. Pang, X. L. Feng, K. Müllen and C. Bubeck, *Chem. Commun.*, 2010, **46**, 6243; (b) H. L. Li, S. P. Pang, S. Wu, X. L. Feng, K. Müllen and C. Bubeck, *J. Am. Chem. Soc.*, 2011, **133**, 9423−9429; (c) J. Chen, S. L. Liu, W. Feng, G. Q. Zhang and F. L. Yang, *Phys. Chem. Chem. Phys.*, 2013, **15**, 5664−5669; (d) L. Y. Cao, H. M. Sun, J. Li and L. H. Lu, *Anal. Methods.*, 2011, **3**, 1587−1594.

13 S. Wang, H. L. Li, S. Li, F. Liu, D. Q. Wu, X. L. Feng and L. X. Wu, *Chem. Eur. J.*, 2013, **19**, 10895 – 10902.

14 D. Zhou and B. H. Han, *Adv. Funct. Mater.*, 2010, **20**, 2717–2722.

15 J. L. Zhang, H. J. Yang, G. X. Shen, P. Cheng, J. Y. Zhang and S. W. Guo, *Chem. Commun.*, 2010, **46**, 1112–1114.

16 (a) A. Rudnitskaya, J. A. F. Gamelas, D. V. Evtuguinc and A. Legin, *New J. Chem.*, 2012, **36**, 1036–1042; (b) Z. L. Wang, Y. Lu, Y. G. Li, S. M. Wang and E. B. Wang, *Chin Sci Bull*, 2012, **57**, 2265-2268.

17 J. F. Shen, B. Yan, M. Shi, H. W. Ma, N. Li and M. X. Ye, *J. Mater. Chem.*, 2011, **21**, 3415–3421.

18 A. Vadivel Murugan, T. Muraliganth, and A. Manthiram, *Chem. Mater.*, 2009, **21**, 5004–5006.

19 X. J. Sang, J. S. Li, L. C. Zhang, Z. M. Zhu, W. L. Chen, Y. G. Li, Z. M. Su and E. B. Wang, *Chem. Commun.*, 2014, **50**, 14678

20 S. Stankovich, D. A. Dikin, R. D. Piner, K. A. Kohlhaas, A. Kleinhammes, Y. Y. Jia, Y. Wu, S. T. Nguyen and R. S. Ruoff , *Carbon*, 2007, **45**, 1558–1565.

21 J. Suárez-Guevara, V. Ruiz and P. Gómez-Romero, *Phys. Chem. Chem. Phys.*, 2014, **16**, 20411-20414.

22 S. Z. Wen, W. Guan, J. P. Wang, Z. L. Lang, L. K. Yan and Z. M. Su, *Dalton Trans.*, 2012, **41**, 4602–4607.

23 Y. Kim and S. Shanmugam, *ACS Appl. Mater. Interfaces*, 2013, **5**, 12197−12204.

24 S. Wang, H. L. Li, L. Y. Zhang, B. Li, X. Cao, G. H. Zhang, S. L. Zhang and L. X. Wu, *Chem. Commun.*, 2014, **50**, 9700-9703.

25 H. L. Li, J. Gupta, S. Wang, N. Zhang and C. Bubeck, *Journal of Colloid and Interface Science*, 2014, **427**, 25-28.

The Assembly of Vanadium (IV)-Substituted Keggin-type Polyoxometalate/Graphene Nanocomposite and its application in photovoltaic system

Dan Xu, Wei-Lin Chen*, Jian-Sheng Li, Xiao-Jing Sang, Ying Lu, Zhong-Min Su and En-Bo Wang *

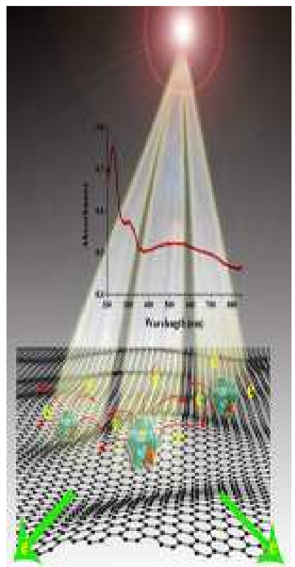

$SiW_{11}V$ in the nanocomposite can absorb nearly full spectrum, the excited electrons of which can be transferred through the graphene.